IEEE Access
Multidisciplinary : Rapid Review : Open Access Journal

Received 10 January 2025, accepted 29 January 2025, date of publication 3 February 2025, date of current version 6 February 2025.

Digital Object Identifier 10.1109/ACCESS.2025.3538054

RESEARCH ARTICLE

Network-Scale Impact of Vegetation Loss on Coverage and Exposure for 5G Networks

JORN SCHAMPHELEER[1], ANKE HUSS[2], AND MARGOT DERUYCK[1], (Member, IEEE)
[1]Department of Information Technology, IMEC, Ghent University, 9052 Ghent, Belgium
[2]Institute for Risk Assessment Sciences, Utrecht University, 3584 CS Utrecht, The Netherlands

Corresponding author: Jorn Schampheleer (jorn.schampheleer@ugent.be)

This work was supported by the Enhancing the Investigation of RF-EMF and its Possible Effects on Human Health and Biodiversity (ETAIN)-Project under Grant 101057216.

ABSTRACT This study investigates the effects of vegetation on 5G network performance, with a particular focus on coverage, user exposure, and base station deployment strategies in an urban environment (Utrecht, The Netherlands). This is the first study to perform network planning simulations that account for vegetation and building-induced propagation challenges on a city-wide scale, providing understanding of their effects on 5G network performance and exposure. The study also explores the influence of user height, examining how vegetation's blocking and shielding effects vary with user height. By evaluating both sub-6 GHz and mmWave networks under various simulated scenarios, the research qualifies the dual role of vegetation as both a coverage barrier and a mitigator of user exposure. Key findings include a significant 14.71% reduction in coverage for sub-6 GHz networks in the presence of vegetation and a 42.98% decrease in downlink whole-body SAR in mmWave networks due to vegetation's shielding effects. Flexible base station placement is shown to effectively counteract coverage losses while maintaining stable exposure metrics, but mmWave networks remain highly sensitive to environmental obstructions. These findings emphasize the importance of incorporating vegetation and other environmental factors into network planning, especially for high-frequency 5G networks, to ensure optimal performance and limit user exposure.

INDEX TERMS 5G network, MaMIMO, mmWave, network planning, vegetation.

I. INTRODUCTION

The fifth generation of mobile networks (5G) introduces significant advancements in telecommunications, offering enhanced capabilities over its predecessors. Designed to provide higher data rates, lower latency, and massive multiple-input multiple-output (MaMIMO) connectivity [1], 5G is a cornerstone of modern telecommunication. Unlike earlier generations, 5G supports higher frequency bands, including millimeter waves, enabling faster data transmission but also presenting new challenges in terms of signal propagation and network reliability.

As the digital landscape evolves towards 6G and beyond, emerging technologies such as the Internet of Things (IoT) [2], smart cities, autonomous vehicles, and advanced healthcare systems will increasingly rely on the robust connectivity provided by 5G networks [3]. These advancements highlight the importance of 5G not just as an upgrade in mobile technology but as a foundational element in the future of global connectivity.

However, the deployment of 5G networks is challenged by environmental factors, particularly those related to signal propagation. The higher frequency bands, while offering benefits in speed and capacity, are more sensitive to physical obstructions such as buildings and vegetation. Vegetation, especially trees, poses a significant challenge due to its potential to cause signal attenuation, scattering, and absorption, leading to a degradation in network performance [4]. These effects are especially underestimated in urban and suburban environments where green spaces and infrastructure coexist.

A. ENVIRONMENTAL OBSTACLES TO 5G SIGNAL PROPAGATION

Buildings are a well-documented source of signal attenuation. Studies such as those by Sorgatz et al. [5], Zhekov et al. [6]

The associate editor coordinating the review of this manuscript and approving it for publication was Xiaodong Xu.

and Bonefačić and Šarolić [7] have quantified signal losses due to building materials, while Rappaport et al. [8] and Shakya et al. [9] compared attenuation models, emphasizing the need for accurate network planning tools. These studies highlight the variability of attenuation based on material properties and signal frequency. Vegetation, while less frequently studied than buildings, also plays a critical role in signal propagation. Vegetative obstructions such as trees can cause attenuation, scattering, and absorption, significantly degrading network performance [4]. Models illustrated by Ma et al. [10], Zhang et al. [11] and Cichoń et al. [12] offer insights into the effects of vegetation on signal loss, while De Beelde et al. [4] and Barb et al. [13] provide a comprehensive overview of vegetation-dependent decay models. These studies underscore the importance of incorporating vegetation effects into network planning, especially in urban areas where green spaces are often overlooked [14]. Atmospheric conditions further compound these challenges. Rain, fog, and gaseous absorption, particularly at higher frequency bands, contribute to significant signal degradation. Hubrechsen et al. [15], Golovachev et al. [16] and Saadoon et al. [17] demonstrate the impact of atmospheric conditions on millimeter-wave and sub-terahertz signals, while Han et al. [18] highlight the specific attenuation effects of rain and oxygen absorption in the 28 GHz to 72 GHz range. Mankong et al. [19] also demonstrated the significance of these effects in backhaul links of 5G networks. An overview of these studies is given in Table 1.

B. RAY TRACERS

Recent advancements in ray tracing techniques, such as Sionna [20], offer detailed modeling of electromagnetic wave propagation, accounting for multidimensional channel characteristics (e.g., amplitude, phase, and polarization) with high precision [21]. However, the reliance on exhaustive geometric and material data presents limitations. Computational intensity further restricts their application to localized, site-specific studies, making them less practical for city-wide exposure-aware network planning at a large scale [22]. By contrast, this study leverages the 3GPP Urban Macro Path Loss Model [23], which is computationally efficient and capable of scalable analysis. While not as detailed as ray tracers, this model provides robust approximations of environmental effects, including vegetation-induced signal attenuation, making it suitable for large-scale urban analyses. This enables a practical approach to integrate exposure-aware planning into 5G deployment strategies.

C. RESEARCH GAP AND OBJECTIVES

Despite the extensive research on individual environmental factors affecting signal propagation, their integration into network planning tools remains limited. For example, while Acuña et al. [14] proposed models for urban network planning, their implementation in practical tools is lacking. Similarly, Dalela et al. [24] used default vegetation loss values without detailed integration into network designs. As a result, the cumulative impact of environmental obstructions on 5G networks, particularly at a city-wide scale, remains underexplored. This study addresses these gaps by providing a comprehensive, network-scale analysis of the effects of vegetation and building-induced attenuation on 5G network performance. By incorporating vegetation into simulations, this research evaluates the dual role of vegetation as both an obstacle to coverage and a mitigator of user exposure. The findings offer valuable insights into optimizing deployment strategies for robust 5G networks. This study is, to the best of our knowledge, the first to implement exposure-aware network planning that explicitly considers the impact of vegetation on 5G network performance, while also considering buildings at city-wide scale.

The novelty of the paper is:

- First to integrate vegetation and building-induced propagation challenges into large city-scale network planning considering both coverage and exposure.
- Evaluates vegetation as both a coverage barrier and an exposure mitigator.
- Highlights adaptive base station placement for balancing coverage and exposure.
- Explores the impact of user height on vegetation's shielding effects.

II. METHODOLOGY

This study builds on the work of Matalatala et al. [25] and Castellanos et al. [26], who developed methods for planning 5G Massive MIMO (MaMiMo) networks with a focus on exposure-aware design. This section details the optimization metrics and the algorithm used for network planning, along with the objective function that accounts for power usage and exposure.

A. PROBLEM DESCRIPTION

Since it was found in found in literature ([27]) that when designing networks, vegetation is quickly overlooked in urban settings, we focused on designing a 5G MaMIMO network for the city of Utrecht in The Netherlands. To design this urban 5G MaMIMO network, three critical objectives must be balanced: maximizing user coverage, minimizing user exposure, and minimizing base station transmit power. The optimization is constrained by operational requirements: base stations must be either active or inactive, adhere to valid power profiles, and support user connections, with each user connecting to at most one base station. Input to this problem is an initial set of base station locations, provided by network operators [28] and a set of 3D building-models, supplied by the Dutch government [29]. Additionally, a Geographic Information System raster (GIS-raster) overlay, detailing tree heights for trees taller than 2.5 meters at a resolution of $5m \times 5m$, is used, also sourced from the Dutch government [30]. For simulating mmWaves, a lamppost dataset is used to generate a list of possible base station locations

TABLE 1. A table illustrating the ongoing research into signal attenuation due to obstacles.

Title	Authors & Year	Blocking Investigated	Summary of Findings
Overview of Millimeter Wave Communications for Fifth-Generation (5G) Wireless Networks—With a Focus on Propagation Models [8]	Rappaport, T. S., et al. (2017)	Buildings	Investigated the challenges of 5G mmWave propagation, finding that building materials significantly impact signal penetration at high frequencies.
Measurement of Attenuation by Building Structures in Cellular Network Bands [6]	Zhekov, S., et al. (2018)	Buildings	Found that modern window materials lead to greater signal attenuation, particularly affecting indoor 5G coverage.
Attenuation of Building Materials and Structures in 5G Millimeter Wave Band [7]	Bonefačić, D. & Šarolić, S. (2023)	Buildings	Measured penetration loss through various building materials. Also noted that blinds significantly attenuate the signal.
Wideband Penetration Loss through Building Materials and Partitions at 6.75 GHz in FR1(C) and 16.95 GHz in the FR3 Upper Mid-band spectrum [9]	Shakya, D., et al. (2024)	Buildings	Compared measurements to 3GPP models for wideband penetration loss through different materials.
Measurements of Building Attenuation in 450 MHz LTE Networks [5]	Sorgatz, et al. (2024)	Buildings	Explored the impact of building-induced blockage in 450 MHz scenarios, showing that newer buildings cause significantly more attenuation due to energy saving materials.
Wireless Wave Attenuation in Forests: An Overview of Models [10]	Ma, Y., et al. (2024)	Vegetation	Lists different models used for vegetation loss in forests. They found that each model has its own strengths and weaknesses.
Measurement-Based 5G Millimeter-Wave Propagation Characterization in Vegetated Suburban Macrocell Environments [11]	Zhang, P., et al. (2020)	Vegetation	Measures foliage blocking in suburban macrocell environments, compares measurements to 3GPP and ITU-R models.
Vegetation Loss Measurements for Single Alley Trees in Millimeter-Wave Bands [12]	Cichoń, K., et al. (2024)	Vegetation	Modelled signal attenuation in a tree alley, developed specific models for the scenario.
Analysis of Vegetation and Penetration Losses in 5G mmWave Communication Systems [13]	Barb, G., et al. (2022)	Vegetation	Studied different models for vegetation loss calculations.
Vegetation Loss at D-Band Frequencies and New Vegetation-Dependent Exponential Decay Model [4]	De Beelde, B., et al. (2022)	Vegetation	Investigates vegetation loss for Fixed Wireless Access (FWA) networks between 110 GHz and 170 GHz.
Millimeter Wave Attenuation Due to Wind and Heavy Rain in a Tropical Region [19]	Mankong, U., et al. (2023)	Weather	Analyzed how heavy rain impacts mmWave links, finding substantial attenuation, particularly affecting backhaul links in 5G networks.
An Overview For The Effects Of Different Weather Conditions On 5G Millimeter Waves Propagations [17]	Saadoon, H. J., et al. (2021)	Weather	Investigated the impact of various weather conditions on 5G mmWave communications, finding rain and fog to be significant sources of attenuation.
The Effect of Weather Conditions on Millimeter Wave Propagation [16]	Golovchev, Y., et al. (2019)	Weather	Investigates the effect of different phases of water in the atmosphere on the propagation of electromagnetic radiation at broadband millimeter wave spectrum.
Atmospheric Attenuation in a mmWave Reverberation Chamber [15]	Hubrechsen, A. (2024)	Weather	Shows how atmospheric conditions can be investigated in reverberation chambers. They found that atmospheric attenuation was especially significant around 54-65 GHz and around 118 GHz.
Impact of Atmospheric Parameters on the Propagated Signal Power of Millimeter-Wave Bands Based on Real Measurement Data [18]	Han, C., Duan, S. (2019)	Weather	Investigates atmospheric attenuation due to rain in LOS conditions based on measurements in China and Göteborg.

mounted on lampposts. This lamppost dataset is also sourced from the Dutch government [31]. Two compressed datasets are created from this lamppost dataset, for performance reasons. One dataset is compressed to include only one lamppost in a radius of 30 meters, to force the optimizer to make compromises. The lampposts are treated in the order they appear, the first lamppost is assumed to be central, all lampposts inside the radius around this first lamppost are removed. This dataset results in 1954 available sites. The second dataset is compressed to include one lamppost in a radius of 25 meters, to allow more freedom during the planning. This extended dataset results in 6208 available sites. A lamppost dataset is chosen due to the availability of the data and the ease of implementation. Since the lamppost base stations can be implemented in any direction and are already placed densely.

The objective function for the network planner is a quad-objective function that simultaneously optimizes user coverage, network power consumption, downlink exposure, and uplink exposure. Exposure limits are based on guidelines from the International Commission on Non-Ionizing Radiation Protection (ICNIRP) [32]. Specifically, downlink exposure is measured by the whole-body specific absorption rate ($SAR_{whole-body}$) with a limit of 0.08 W/kg, while uplink exposure depends on the signal frequency. For frequencies up to 6 GHz, the localized specific absorption rate (SAR_{local}) with a limit of $2W/kg$ is used. For frequencies above 6 GHz,

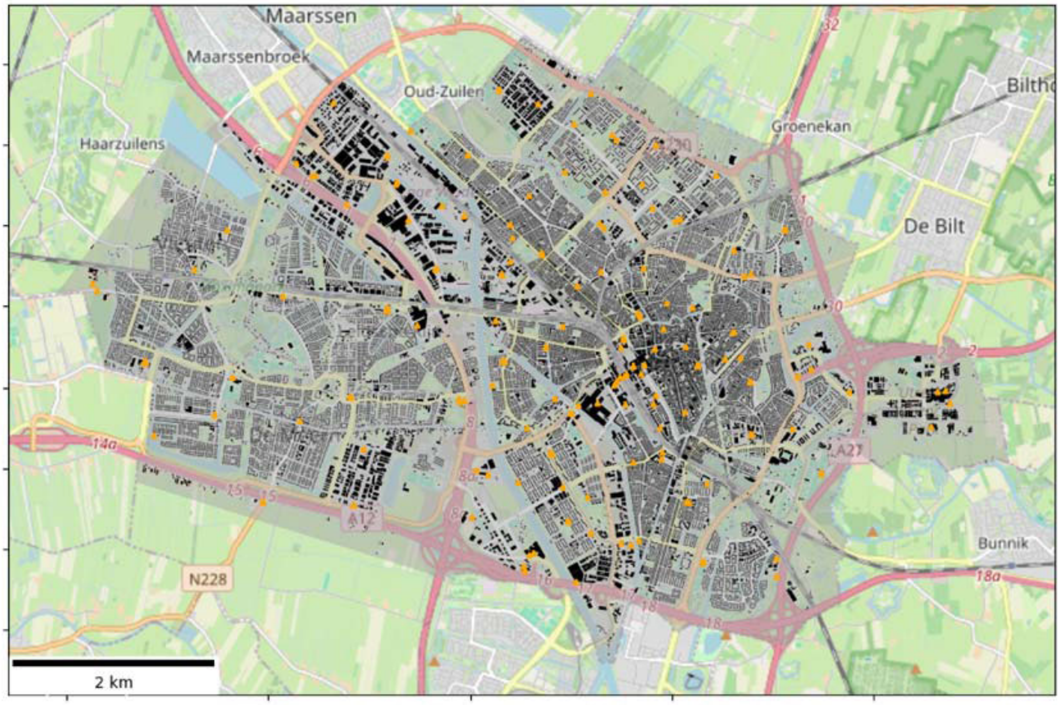

FIGURE 1. City of Utrecht, The Netherlands, with possible base station locations (orange triangles) [33].

the localized absorbed power density (Sab_{local}) with a limit of $20W/m^2$ is applied.

B. SIMULATION SETUP

The network planning algorithm requires input data to define the initial evaluation scenario from which optimization begins. Fig. 1 shows the simulation area with existing buildings (gray background with black structures) and potential base station locations (orange triangles). 169 unique base station sites are available. For the initial base station locations, three frequencies are simulated: 800 MHz, 2100 MHz and 3500 MHz. For the base stations supporting 3500 MHz, MaMiMo is enabled. For the mmWave lamppost base stations, only 28 GHz is supported.

Since the algorithm is capacity-based, it proceeds by populating this scenario with users, whose exposure and coverage are then optimized. Users are distributed based on Utrecht's population density, using a cumulative distribution function (CDF) at the neighbourhood level [30]. A total of 2115 users is simulated, according to operator network usage data. Each user is randomly positioned in an outside location according to the weighted CDF and assigned a bitrate request, which determines the minimum required link speed.

C. ALGORITHM OVERVIEW

At the start, the available data includes a set of base stations $\beta = \{1, 2, \ldots, M\}$ and users $\Upsilon = \{1, 2, \ldots, N\}$. The binary variable x_{mn} is introduced to indicate whether a user is connected to a base station, as shown in Eq. 1.

$$x_{mn} = \begin{cases} 1, & \text{if the n-th user is connected to the m -th BS} \\ 0, & \text{otherwise.} \end{cases} \tag{1}$$

Similarly, the binary variable y_m indicates whether a base station is active, as defined in Eq. 2.

$$y_m = \begin{cases} 1, & \text{if BS m is active} \\ 0, & \text{otherwise.} \end{cases} \tag{2}$$

The discrete variable p_m, representing the transmission power of the m-th base station, is defined as $p_m \in \{0, 1, 2, \ldots, p_t\}$, where p_t is the maximum supported transmission power for this base station. The solution vector thus includes variables indicating whether a base station is active, its operating power in dBm, and the users connected to it.

To optimize these variables, an objective function is defined (Eq. 3) that is minimized across all base stations, users, and power settings. Scaling factors ω assign priorities to different objectives, with default values of $\omega_1 = 1.0$, $\omega_2 = 0.2$, $\omega_3 = 0.4$, and $\omega_4 = 0.4$, prioritizing user coverage over exposure and then power consumption.

$$F(m, n) = \left(\frac{-\omega_1 \sum_{m \in \beta, n \in \Upsilon} x_{nm}}{N} \right) + \left(\frac{\omega_2 \sum_{m \in \beta} P_{\text{calc}}\left(y_m p_m\right)}{P_{\max}} \right)$$

$$+\left(\frac{\omega_3 \sum_{m\in\beta,n\in\Upsilon} Exp_{\mathrm{ul}}\left(x_{mn}y_m\right)}{Exp_{ul,\max}}\right)$$
$$+\left(\frac{\omega_4 \sum_{m\in\beta,n\in\Upsilon} SAR_{\mathrm{dl,\ n}}\ \left(y_m\right)}{SAR_{dl,\max}}\right) \tag{3}$$

The choice is made to make the objective function optimal when minimized. The first term in Eq. 3 rewards successful user connections, normalized by the total number of users Each connected user contributes to lowering the objective function that is optimal when minimized. The second term penalizes higher power usage, where P_{calc} is the calculated power consumption of the network, normalized by the network's maximum possible power usage [34]. Each base station that is on and transmitting increases the objective function depending on how much power is transmitted. The third term penalizes high uplink exposure (Eq. 4), calculated either as SAR (Eq. 5) or Sab (Eq. 6), depending on frequency. For each user the uplink SAR is summed. Higher uplink exposure increases the objective function more than lower exposure. This exposure depends on the uplink duty cycle of the Time Division Duplex (TDD) network mode, assumed to be 0.25 as proposed by Thors et al. [35], and on the required signal power (P_{act}, Eq. 7) for communication, based on receiver sensitivity and path loss. Finally, the fourth term penalizes higher downlink exposure, calculated for each user based on the incident power densities across all base stations multiplied by the downlink SAR conversion factor (SAR^{DL}_{ref}), the duty cycle of the TDD network mode (assumed to be 0.75 as in Castellanos et al. [26]), and the spatial duty cycle ([35], [36]), as demonstrated in Eq. 8. The downlink SAR is calculated in each user and summed, which causes the objective function to increase more for higher downlink SAR.

$$Exp_{ul} = \begin{cases} SAR_{ul}, & \text{iff } \le 6\text{GHz} \\ Sab_{ul}, & \text{iff } > 6\text{GHz} \end{cases} \tag{4}$$
$$SAR_{ul} = P_{act} \cdot DC^{UL}_{TDD} \cdot SAR^{UL}_{ref} \qquad [\mathrm{W\,kg^{-1}}] \tag{5}$$
$$Sab_{ul} = P_{act} \cdot DC^{UL}_{TDD} \cdot Sab^{UL}_{ref} \qquad [\mathrm{W\,m^{-2}}] \tag{6}$$
$$P_{act} = 10^{\frac{\max(-26,\min(rxsens+PL,23))-30}{10}} \qquad [\mathrm{W}] \tag{7}$$
$$SAR_{dl,n} = SAR^{dl}_{ref} \cdot \sum_{m\in\beta} S_{BS_m} \cdot DC^{DL}_{TDD} \cdot DC^{DL}_{SPA} \qquad [\mathrm{W\,kg^{-1}}] \tag{8}$$

More specifically, Eq. 5 represents the Specific Absorption Rate (SAR) to which a user is exposed due to uplink traffic. It is determined by three key factors: the power (P_{act}) required by the User Equipment (UE) to communicate with the base station at the specified bitrate; the uplink duty cycle (DC^{UL}_{TDD}) of the Time Division Duplex (TDD) network mode, which accounts for the proportion of time the UE transmits in this mode; and the uplink SAR (SAR^{UL}_{ref}) in watts per kilogram (W/kg) for 1 W of transmitted power at the specific frequency.

Similarly, Eq. 6 calculates exposure as Specific Absorption per Unit Area (Sab) for frequencies above 6 GHz. It uses the uplink Sab (Sab^{UL}_{ref}) in watts per square meter (W/m^2) for 1 W of transmitted power at the specific frequency.

The actual transmit power of the user's device, P_{act}, is illustrated in Eq. 7 and ranges from -26 to 23 dBm. This power depends on the propagation path loss (PL) experienced by the user (in dB) and the sensitivity of the base station (*rxsens*) in dBm, which is required to maintain the user's bitrate.

Lastly, Eq. 8 describes the downlink SAR. The downlink SAR at a given point is determined by summing the incident power densities (S_{BS_m}) contributed by each base station m. These values are adjusted by the downlink duty cycle (DC^{DL}_{TDD}) of the TDD mode and the spatial duty cycle (DC^{DL}_{SPA}) of the base station's beam. The summed value is then multiplied by the downlink SAR conversion factor (SAR^{DL}_{ref}), which represents the whole-body SAR in watts per kilogram (W/kg) for 1 W of transmitted power.

D. FORMAL DEFINITION

Based on the variables defined in Section II-C, the optimization problem can be formally defined as follows:

$$\begin{aligned} &\min_{m,n} \quad F(m,n) \\ &\text{s.t.} \\ &\quad C_1 : y_m \in 0, 1, \forall m \in \beta \\ &\quad C_2 : p_m \in 0, 1, 2, \cdots, p_t, \forall m \in \beta \\ &\quad C_3 : x_{mn} \in 0, 1, \forall n \in \Upsilon, \forall m \in \beta \\ &\quad C_4 : \sum_{m=1}^{\beta} x_{mn} = 1, \forall n \in \Upsilon, \forall n \in \beta \end{aligned}$$

The goal is to minimize the objective function defined in Eq. 3, subject to the following constraints: C1 ensures that a base station is either active or inactive, C2 governs the transmission power, C3 represents the association between base stations and users, and C4 limits each user to connecting with only one base station. Since each variable in this problem is integer based, and since this problem is subjected to constraints with an objective function, it is defined as a Mixed Integer Problem (MIP). To solve this problem, a MIP-solver can be used such as Gurobi [37], which is used in this study.

E. PATH LOSS

A connection between a user and a base station is viable only if the path loss along the link does not exceed the required signal strength to meet the user's bitrate request. Various obstacles, such as buildings, atmospheric conditions, and vegetation, can impede the signal, as outlined in Section I. Even in a Line of Sight (LoS) scenario, environmental factors can still cause signal attenuation.

The 3rd Generation Partnership Project (3GPP) has developed several models to accurately simulate path loss in urban environments [23]. For this study, the 3GPP 38.900 Urban Macro (UMa) and Urban Micro (UMi) models are particularly relevant. The UMa model is designed for macrocell base stations in urban areas, while the UMi model focuses on microcells, often situated in street canyons. These models account also for losses due to scattering from buildings, with empirical data supporting their use. Although the 3GPP also provides models for outdoor-to-indoor (O2I) building losses, these are less relevant for this study since all users are simulated outdoors.

As discussed in the literature review (Section I), De Beelde et al. [4] compared various vegetation loss models, identifying the Weissberger model as the most versatile in terms of applicable frequency and distance ranges. The Weissberger model is defined by the loss function in Eq. 9, where f represents the frequency (in GHz), and d denotes the depth of the vegetation (in m).

$$L_{\text{Weissberger}}(f, d) = \begin{cases} 0.45 \cdot f^{0.284} \cdot d, & d \in [0, 14]\text{m} \\ 1.33 \cdot f^{0.284} \cdot d^{0.588}, & d \in [14, 400]\text{m} \end{cases} \tag{9}$$

When calculating vegetation loss in the network planner, two important considerations must be taken into account: height and distance. Although the Weissberger formula does not explicitly include height as a variable, the height of the vegetation affects the proportion of the signal that travels through it, as illustrated in Figure 2. Moreover, the distance that the signal travels through the vegetation significantly influences the overall loss.

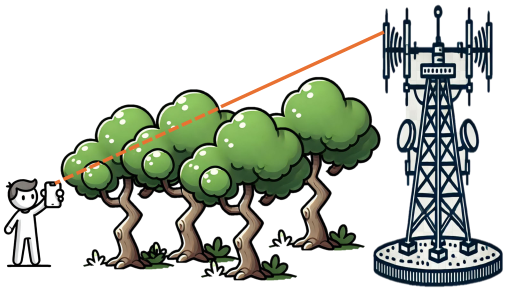

FIGURE 2. Connection between a user and a base station partially propagating through vegetation.

The GIS-raster used in this study, shown in Figure 3, provides a 5m x 5m resolution map of tree heights for all trees taller than 2.5 meters, as provided by the Dutch government [30]. This raster allows calculating the distance a signal travels through vegetation, enabling estimation of signal attenuation using the Weissberger model.

The final path loss is thus the sum of the attenuation calculated using the appropriate 3GPP UMa or UMi path loss model and the vegetation loss derived from the Weissberger model. No rain is assumed in this study.

F. NETWORK PARAMETERS

Additional parameters crucial for the simulation are listed in Table 2. These values are primarily derived from Castellanos et al. [26] and are extended to include the 28 GHz frequency band for mmWave simulations.

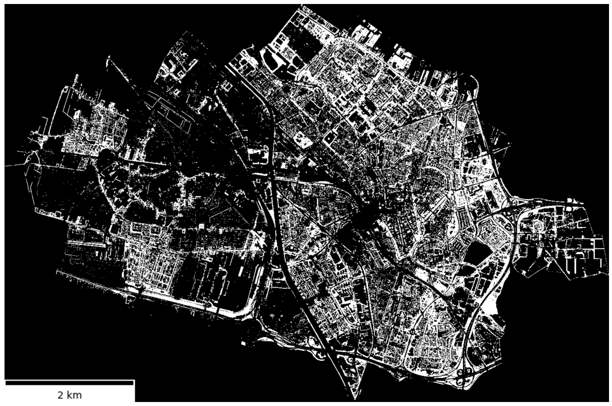

FIGURE 3. The vegetation raster file, including trees taller than 2.5m and their height [30].

G. SIMULATION OUTPUT

After defining the objective function and calculating the path loss for each potential connection Gurobi is employed to solve the network planning problem. The output consists of the values of y_m, x_{mn}, and p_m, indicating which users are connected to which base stations, as well as the transmission power settings for each base station.

Based on these outputs and using the equations from Section II, the network's power consumption can be calculated through P_{calc}. Similarly, uplink and downlink exposure metrics are determined using Exp_{ul} and SAR_{dl}, respectively.

To ensure the robustness of the results, the simulation is repeated 40 times, as suggested in Deruyck et al. [38], with averages taken for all key metrics. For some metrics, like exposure, percentiles are also reported to show how they relate to the entire user population. For example, P99 SAR refers to the 99th percentile of reported SAR exposures. The repetition of the simulations accounts for the spatially random distribution of users in each simulation run, reducing the potential impact of outliers on the final analysis.

H. SIMULATION SCENARIO'S

After defining te required formula's, the simulation scenario's can be defined. The first scenario is a comparison of the initial evaluation scenario, with and without vegetation. The second scenario extends this first scenario, by using an extended list of base stations. The original scenario has 169 available base station locations and is based on operator data, whereas the second scenario has 469 available base station locations. This list is generated based on the original list, extended with possible base station locations that are at least 15 meters (the defined safety distance) from buildings. The third scenario evaluates the influence of the height of the user on the effects of the vegetation. In the fourth scenario a comparison is made specifically for a mmWave network, with and without vegetation. This is done using the base station locations list generated from the compressed lamppost dataset, featuring 1954 available sites. Lastly, in the fifth scenario the same comparison is made as in the fourth scenario, but this time

TABLE 2. Network parameters used for the simulation of 5G NR mobile networks [26].

Parameter	Unit	5G 800	5G 2100	5G 3500	5G 28000
Band					
Simulated frequency	MHz	800	2100	3500	28000
Channel bandwidth (max available)	MHz	120	120	120	400
Sampling factor	–	1536	1536	1536	1536
TDD duty cycle dl	%	75	75	75	75
TDD duty cycle ul	%	25	25	25	25
Spatial duty cycle	%	0	0	15	5
TX/RX					
BS transmit antenna gain (total)	dBi	16	18	24	28
BS transmit array antenna feed loss	dB	2	2	2	0
BS total radiated power (new sites)	dBm	46	49	53	33
BS number of antenna elements	#	1	1	64	192
MS receive antenna element gain	dBi	0	0	0	6
MS transmit power	dBm	23	23	23	6
MS antenna height	m	1.5	1.5	1.5	1.5
MS number of antenna elements	#	1	1	1	4
RX noise figure	dB	8	8	7	8
Propagation					
Path loss model	–	TR 38.901	TR 38.901	TR 38.901	TR 38.901
Low building loss (70%)	dB	12.4	12.6	12.9	17.6
High building loss (30%)	dB	30.2	30.6	30.6	37.6
Other losses (shadow, fading)	dB	22.8	25.2	20	22.8
Safety distance (user-bs)	m	15	15	15	15
SNR					
SNR required for 100 Mbps	dB	0 @120 MHz	0 @120 MHz	0 @120 MHz	-3 @400 MHz
SNR required for 1 Gbps	dB	27 @120 MHz	27 @120 MHz	27 @120 MHz	3 @400 MHz

with the extended lamppost dataset featuring 6208 available sites. Each scenario compares network planning outcomes with and without vegetation considerations to underline the importance of including vegetation in network simulations. These scenarios are reflective of practical planning decisions in current network deployments, demonstrated in an urban setting where vegetation planning is usually overlooked.

III. RESULTS

This section presents the outcomes of the conducted study.

A. SCENARIO 1: EVALUATING INITIAL SETUP

In the first scenario, a 5G simulation was conducted in Utrecht using the base station locations provided by operators. The comparison is made between simulations with and without vegetation present. The UMa path loss model was employed in both cases, with user bitrate requests set at 100 Mbps, a typical speed in 5G networks [39]. The results, averaged over 40 simulation runs, are summarized in Table 3.

Although both scenarios used approximately the same number of base stations, the presence of vegetation had a significant impact on network coverage. Without considering vegetation, 14.71% of the users (311 users) would be unable to connect to the network. Furthermore, uplink exposure increases as users must transmit at higher power levels to maintain a connection through vegetation, which leads to increased uplink exposure from handheld devices.

A shift in the utilized frequencies can be seen in Fig. 4, where the model shows a preference for lower frequencies due to their superior penetration capabilities. Notably, there is a 20% decrease in the use of the 3500 MHz band as more 800 MHz base stations are favored, while the usage of 2100 MHz remains unchanged. The objective function clearly favors the 800 MHz frequency. This preference arises because the objective function seeks to optimize both coverage and exposure. Lower frequencies experience less attenuation from obstacles, allowing a single base station to serve more users, provided the signal-to-noise ratio (SNR) is high enough to maintain the required bitrate. As a result, fewer base stations are needed, reducing exposure while maintaining or even improving coverage. However, as the required bitrate increases, the model would be compelled to shift towards higher frequencies, as they can support the higher data rates necessary for demanding applications.

Conversely, the downlink exposure decreases due to vegetation. The base stations reduce their transmission power as users who were difficult to reach without vegetation become unreachable due to the additional attenuation. As a result, the downlink exposure for nearby users is reduced. Figures 5 and 6 visually represent this difference, clearly showing reduced downlink exposure in Fig. 6. The simulation confirms that downlink exposure decreased by nearly 20%.

B. SCENARIO 2: EXTENDED BASE STATION LIST

In the previous scenario, it was observed that the model utilized nearly all available base stations, yielding limited flexibility. Therefore, the scenario was repeated with 469 base station sites available. Table 4 presents the results.

The increased number of available sites resulted in enhanced network coverage, reaching 96.67% without vegetation and 97.11% with vegetation. The improvement in coverage with vegetation is due to the deployment of 13.43%

TABLE 3. Simulation results for a 5G network in Utrecht with 2115 users and a bitrate request of 100 Mbps.

Metric	No vegetation	Vegetation	Percent difference
Number of base stations	147	146	-0.31%
Coverage (based on users, in %)	82.60	70.44	-14.71%
P99 SAR_UL (W/Kg)	0.10	0.11	8.98%
P99 SAR_DL (μW/Kg)	0.26	0.20	-19.99%

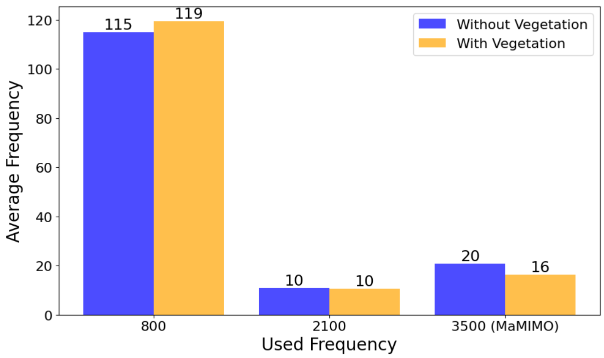

FIGURE 4. Histogram of used frequencies without vegetation versus with vegetation, showing the average deployments per frequency.

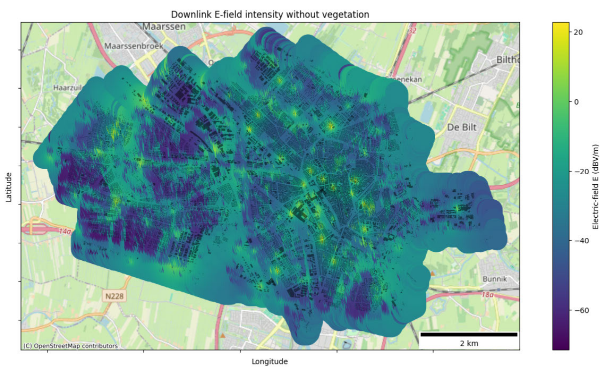

FIGURE 5. Downlink E-field intensity map without vegetation showing intensity 1.5 meters above ground.

more base stations (on average, 27 additional base stations). The uplink SAR remained relatively unchanged, likely because the denser base station deployment balanced out the increased power needed to penetrate vegetation. Similarly, although downlink SAR decreased with the introduction of vegetation, the reduction was smaller than in Scenario 1 (19.99% in Scenario 1 versus 6.67% in Scenario 2), as the additional base stations naturally increased downlink exposure.

C. SCENARIO 3: IMPACT OF USER HEIGHT

To examine the impact of user height above the ground on network performance, the height of simulated users was varied to simulate different floors in buildings, with each floor assumed to be 2.6 meters high [40]. Fig. 7 shows that as user height increases, downlink exposure also rises (on average 1.44 μW/kg increase per m between 4 m and 16 m). A slight increase is observed up to 4.1 meters, just below the 25th percentile of tree heights at 5.3 meters, followed by a sharper rise.

As users approach the base station antenna, the distance decreases, leading to higher exposure due to reduced attenuation. Uplink exposure, however, remains constant at P99 across all heights, indicating that it is primarily determined by users at the cell's edge. The P90 uplink exposure shows a downward trend in Fig. 8 (on average 2.55 mW/kg decrease per m between 0 m and 10 m), slowing around 9.3 meters, corresponding to the 75th percentile of tree heights, where fewer trees exceed this height.

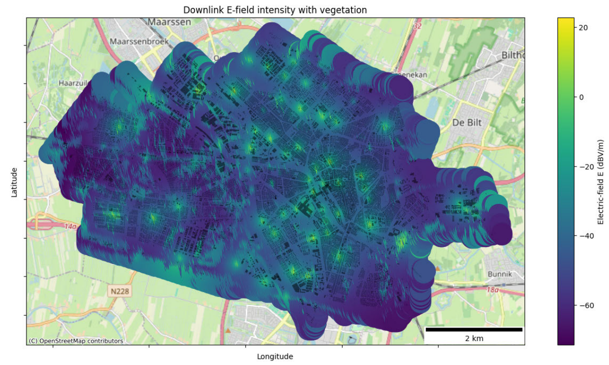

FIGURE 6. Downlink E-field intensity map with vegetation showing intensity 1.5 meters above ground.

TABLE 4. Simulation results for a 5G network in Utrecht with 2115 users and a bitrate request of 100 Mbps, using an extended base station location list.

Metric	No vegetation	Vegetation	Percent difference
Number of base stations	198.48	225.13	13.43%
Coverage (based on users, in %)	96.67	97.11	0.46%
P99 SAR_UL (W/Kg)	0.03	0.03	-0.51%
P99 SAR_DL (μW/Kg)	0.30	0.28	-6.67%

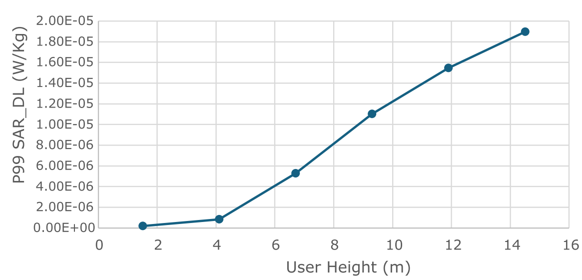

FIGURE 7. P99 downlink SAR considering user height.

D. SCENARIO 4: IMPACT OF VEGETATION ON MMWAVE NETWORKS

For the fourth scenario, the impact of vegetation on a 28GHz mmWave network with lamppost-mounted base stations was

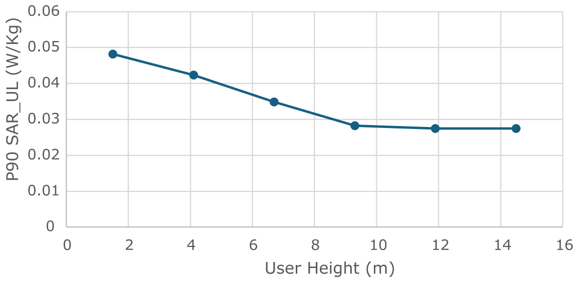

FIGURE 8. P90 uplink SAR considering user height.

investigated, as shown in Table 5. For this scenario the 3GPP UMi path loss model is used, and a bitrate request of 100 Mbps is kept. The simulations show that the number of base stations required remains similar at respectively 315 and 313 base stations used with and without vegetation, and the coverage only drops by 3% when vegetation is considered. However, coverage without vegetation was only 84.22%, and 81.57% with vegetation, highlighting the line-of-sight dependency of mmWave signals.

Uplink exposure remains constant, as users rely on line-of-sight connections. Interestingly, downlink SAR decreased by 42.98% due to vegetation shielding users from exposure to other base stations. This scenario underscores the importance of network planning that takes vegetation into account.

Additionally, since the same number of base stations was used both with and without the presence of vegetation, it indicates that the optimizer had to balance coverage across a limited number of base stations, focusing on ensuring line-of-sight connections to as many users as possible.

TABLE 5. Simulation results for a 5G mmWave network in Utrecht with 2115 users and a bitrate request of 100 Mbps, using lamppost-mounted base stations.

Metric	No vegetation	Vegetation	Percent difference
Number of base stations	315	313	-0.69%
Coverage (based on users, in %)	84.22	81.57	-3.14%
P99 Sab_UL (mW/m^2)	3.74	3.74	0%
P99 SAR_DL (μW/Kg)	0.23	0.13	-42.98%

E. SCENARIO 5: EXTENDED MMWAVE BASE STATION LIST

In the fifth scenario, the list of potential base station locations was extended to assess the network's behavior when there are no restrictions on available sites. Table 6 presents the results of this scenario. Despite having more base station locations to choose from, the simulations still utilized a similar number of base stations, highlighting the constraints imposed by mmWave technology.

In contrast to the previous scenario, the network without vegetation achieved a much higher coverage rate of 96.48%, while the presence of vegetation reduced coverage to 87.89%, representing an 8.9% decrease. This significant drop in coverage underscores the critical impact of vegetation on mmWave networks, where line-of-sight connections are essential. It demonstrates that even with an extended base station list, an all-mmWave network cannot fully compensate for the effects of vegetation, emphasizing the need for careful consideration of natural obstructions in network planning.

TABLE 6. Simulation results for a 5G mmWave network in Utrecht with 2115 users and a bitrate request of 100 Mbps, using an extended list of lamppost-mounted base stations.

Metric	No vegetation	Vegetation	Percent difference
Number of base stations	618.18	641.73	3.81%
Coverage (based on users, in %)	96.48	87.89	-8.90%
P99 Sab_UL (W/m2)	6.24	6.24	0.00%
P99 SAR_DL (μW/Kg)	0.04	0.03	-17.71%

F. COMPARISON WITH PREVIOUS WORK

The exposure metrics observed in this study are of the same order of magnitude as the results reported in [25], [26], [41], [42]. An important remark is that in Castellanos et al. [26] it was found that the uplink SAR was multiple factors higher than the downlink. Likewise in Matalatala et al. [25] and in this study, the uplink SAR is always higher than the downlink SAR. Logically, this means that keeping the uplink SAR down is important for keeping user exposure down. Based on the findings in the five investigated scenario's it is shown that by adding more base stations, the uplink SAR can be lowered. Additionally, since considering vegetation shows that some of the downlink will be absorbed by the vegetation, the impact of adding more base stations on the downlink is lower than estimated in other studies. Limitations of this study include the assumption of a unique network provider. In a real scenario the sites of the simulation would need to be divided amongst providers, ensuring each provider has appropriate coverage.

IV. CONCLUSION

This study examined the impact of vegetation on 5G networks through various simulated scenarios, revealing significant findings regarding network performance, user coverage, and exposure metrics. In the first scenario, where the base station locations were fixed, the presence of vegetation led to a substantial decrease in user coverage, with 14.71% of users unable to connect. Additionally, uplink exposure increased due to the greater power needed to reach base stations, while downlink exposure decreased as unreachable users were removed from the network's coverage area. These findings highlight the importance of incorporating vegetation effects into network planning.

In the second scenario, allowing for a more flexible base station deployment resulted in improved coverage, with minimal differences between the cases with and without vegetation. The increased number of base stations mitigated the negative impact of vegetation, keeping uplink SAR stable while reducing downlink SAR. This demonstrates that a denser base station deployment can alleviate coverage and exposure issues caused by environmental factors such as vegetation.

The third scenario demonstrated the effect of user height on downlink exposure, showing that as users rise above the vegetation canopy, downlink exposure increases due to reduced obstruction and proximity to the base station. Uplink exposure, however, decreased as users moved higher, as vegetation effects diminished and distance to the base station decreased.

The impact of vegetation on mmWave networks was studied in the fourth scenario. Despite the fixed number of base stations in the mmWave scenario, vegetation still caused a reduction in coverage, though to a lesser degree compared to sub-6 GHz networks due to the flexible deployment of mmWave microcell base stations. However, vegetation provided significant shielding from downlink exposure, reducing downlink SAR by 42.98%.

In the fifth scenario, the list of possible base station locations was extended to investigate how the network behaves without restrictions on base station placement. Even with a greater number of available base stations, vegetation still resulted in a coverage drop of 8.9% (188 users), highlighting the persistent challenges of achieving optimal coverage in an all-mmWave network when natural obstructions like vegetation are present. This emphasizes the necessity of considering vegetation when designing high-frequency networks.

In conclusion, the results of this study demonstrate that vegetation significantly affects both the coverage and exposure metrics in 5G networks, particularly in scenarios with fixed base station locations. However, increasing the number of base stations can mitigate some of these effects, especially in urban environments. Additionally, planning for higher-frequency networks, such as mmWave, must account for vegetation's impact on signal propagation and user exposure. Overall, careful network design considering environmental factors such as vegetation is essential for optimizing both network performance and user exposure in 5G networks.

REFERENCES

[1] T. L. Marzetta, E. G. Larsson, H. Yang, and H. Q. Ngo, *Fundamentals of Massive MIMO*. Cambridge, U.K.: Cambridge Univ. Press, 2016. [Online]. Available: https://www.cambridge.org/core/books/fundamentals-of-massive-mimo/C43AF993A6DA7075EC5F186F6BAC914B

[2] L. E. Talavera, M. Endler, I. Vasconcelos, R. Vasconcelos, M. Cunha, and F. J. d. S. e. Silva, ''The mobile hub concept: Enabling applications for the Internet of Mobile Things,'' in *Proc. IEEE Int. Conf. Pervasive Comput. Commun. Workshops (PerCom Workshops)*, Mar. 2015, pp. 123–128. [Online]. Available: https://ieeexplore.ieee.org/document/7134005/?arnumber=7134005

[3] R. Dangi, P. Lalwani, G. Choudhary, I. You, and G. Pau, ''Study and investigation on 5G technology: A systematic review,'' *Sensors*, vol. 22, no. 1, p. 26, Dec. 2021. [Online]. Available: https://www.ncbi.nlm.nih.gov/pmc/articles/PMC8747744/

[4] B. De Beelde, R. De Beelde, E. Tanghe, D. Plets, K. Verheyen, and W. Joseph, ''Vegetation loss at D-band frequencies and new vegetation-dependent exponential decay model,'' *IEEE Trans. Antennas Propag.*, vol. 70, no. 12, pp. 12092–12103, Dec. 2022. [Online]. Available: https://ieeexplore.ieee.org/document/9906796/?arnumber=9906796&tag=1

[5] C. Sorgatz, C. Lüders, and M. Rademacher, ''Measurements of building attenuation in 450 MHz LTE networks,'' 2024, *arXiv:2405.09344*.

[6] S. S. Zhekov, Z. Nazneen, O. Franek, and G. F. Pedersen, ''Measurement of attenuation by building structures in cellular network bands,'' *IEEE Antennas Wireless Propag. Lett.*, vol. 17, pp. 2260–2263, 2018. [Online]. Available: https://ieeexplore.ieee.org/document/8476174

[7] D. Bonefacic and L. Šarolic, ''Attenuation of building materials and structures in 5G millimeter wave band,'' in *Proc. 17th Eur. Conf. Antennas Propag. (EuCAP)*, Mar. 2023, pp. 1–5. [Online]. Available: https://ieeexplore.ieee.org/abstract/document/10133555

[8] T. S. Rappaport, Y. Xing, G. R. MacCartney, A. F. Molisch, E. Mellios, and J. Zhang, ''Overview of millimeter wave communications for fifth-generation (5G) wireless networks—With a focus on propagation models,'' *IEEE Trans. Antennas Propag.*, vol. 65, no. 12, pp. 6213–6230, Dec. 2017. [Online]. Available: https://ieeexplore.ieee.org/document/7999294

[9] D. Shakya, M. Ying, T. S. Rappaport, H. Poddar, P. Ma, Y. Wang, and I. Al-Wazani, ''Wideband penetration loss through building materials and partitions at 6.75 GHz in FR1(C) and 16.95 GHz in the FR3 upper mid-band spectrum,'' 2024, *arXiv:2405.01362*.

[10] Y. Ma, W. Li, D. Han, Y. He, Q. Li, X. Bai, and D. Xu, ''Wireless wave attenuation in forests: An overview of models,'' *Forests*, vol. 15, no. 9, p. 1587, Sep. 2024. [Online]. Available: https://www.mdpi.com/1999-4907/15/9/1587

[11] P. Zhang, B. Yang, C. Yi, H. Wang, and X. You, ''Measurement-based 5G millimeter-wave propagation characterization in vegetated suburban macrocell environments,'' *IEEE Trans. Antennas Propag.*, vol. 68, no. 7, pp. 5556–5567, Jul. 2020. [Online]. Available: https://ieeexplore.ieee.org/document/9014521

[12] K. Cichoń, M. Nikiforuk, and A. Kliks, ''Vegetation loss measurements for single alley trees in millimeter-wave bands,'' *Sensors*, vol. 24, no. 10, p. 3190, May 2024. [Online]. Available: https://www.mdpi.com/1424-8220/24/10/3190

[13] G. Barb, F. Danuti, M. A. Ouamri, and M. Otesteanu, ''Analysis of vegetation and penetration losses in 5G mmWave communication systems,'' in *Proc. Int. Symp. Electron. Telecommun. (ISETC)*, Nov. 2022, pp. 1–5. [Online]. Available: https://ieeexplore.ieee.org/document/10009963

[14] J. E. Acuña, I. Cuiñas, P. Gömez, and M. G. Sánchez, ''Urban cellular network planning imbalances in wooded streets and parks [wireless corner],'' *IEEE Antennas Propag. Mag.*, vol. 53, no. 5, pp. 197–204, Oct. 2011. [Online]. Available: https://ieeexplore.ieee.org/abstract/document/6138469

[15] A. Hubrechsen, L. A. Bronckers, A. C. F. Reniers, and A. B. Smolders, ''Atmospheric attenuation in a mmWave reverberation chamber,'' *IEEE Antennas Wireless Propag. Lett.*, vol. 23, pp. 1730–1733, 2024. [Online]. Available: https://ieeexplore.ieee.org/abstract/document/10440405

[16] Y. Golovachev, A. Etinger, G. A. Pinhasi, and Y. Pinhasi, ''The effect of weather conditions on millimeter wave propagation,'' *Int. J. Circuits, Syst. Signal Process.*, vol. 13, pp. 690–695, Dec. 2019.

[17] H. Saadoon, T. Jamel, and H. Khazal, ''An overview for the effects of different weather conditions on 5G millimeter waves propagations,'' in *Proc. 3rd Conf. Post Graduate Researches Graduation (CPGR)*, Iraq, Oct. 2021. [Online]. Available: https://www.researchgate.net/publication/355336708_An_Overview_For_The_Effects_Of_Different_Weather_Conditions_On_5G_Millimeter_Waves_Propagations_yt_ajlw_alzrwf_at_thry_ta_yl_amt_nzrt_ml_a_amlwjat_ntshar_a_yl_akhmltlft_myt_l_mn_yt_akhlams_ajlyl

[18] C. Han and S. Duan, ''Impact of atmospheric parameters on the propagated signal power of millimeter-wave bands based on real measurement data,'' *IEEE Access*, vol. 7, pp. 113626–113641, 2019. [Online]. Available: https://ieeexplore.ieee.org/abstract/document/8787789

[19] U. Mankong, P. Chamsuk, S. Nakprasert, S. Potha, Z.-K. Weng, P. T. Dat, A. Kanno, and T. Kawanishi, ''Millimeter wave attenuation due to wind and heavy rain in a tropical region,'' *Sensors*, vol. 23, no. 5, p. 2532, Feb. 2023. [Online]. Available: https://www.mdpi.com/1424-8220/23/5/2532

[20] J. Hoydis, S. Cammerer, F. A. Aoudia, A. Vem, N. Binder, G. Marcus, and A. Keller, ''Sionna: An open-source library for next-generation physical layer research,'' 2022, *arXiv:2203.11854*.

[21] J. Hoydis, F. Aït Aoudia, S. Cammerer, M. Nimier-David, N. Binder, G. Marcus, and A. Keller, "Sionna RT: Differentiable ray tracing for radio propagation modeling," 2023, *arXiv:2303.11103*.
[22] K. Guan, D. He, T. Kürner, and Z. Zhong, "To know channels better: Challenges and opportunities of ray tracing," in *Proc. 17th Eur. Conf. Antennas Propag. (EuCAP)*, Mar. 2023, pp. 1–3. [Online]. Available: https://ieeexplore.ieee.org/document/10133671
[23] (2018). *Specification # 38.900*. [Online]. Available: https://portal.3gpp.org/desktopmodules/Specifications/SpecificationDetails.aspx?specificationId=2991
[24] P. Dalela, M. Prasad, and A. Mohan, "A new method of realistic GSM network planning for rural Indian terrains," *Int. J. Comput. Sci. Netw. Secur.*, vol. 8, no. 8, Aug. 2008. [Online]. Available: http://paper.ijcsns.org/07_book/html/200808/200808052.html
[25] M. Matalatala, M. Deruyck, S. Shikhantsov, E. Tanghe, D. Plets, S. Goudos, K. E. Psannis, L. Martens, and W. Joseph, "Multi-objective optimization of massive MIMO 5G wireless networks towards power consumption, uplink and downlink exposure," *Appl. Sci.*, vol. 9, no. 22, p. 4974, Nov. 2019. [Online]. Available: http://hdl.handle.net/1854/LU-8640468
[26] G. Castellanos, S. De Gheselle, L. Martens, N. Kuster, W. Joseph, M. Deruyck, and S. Kuehn, "Multi-objective optimisation of human exposure for various 5G network topologies in Switzerland," *Comput. Netw.*, vol. 216, Oct. 2022, Art. no. 109255. [Online]. Available: https://www.sciencedirect.com/science/article/pii/S1389128622003231
[27] I. Cuinas, P. Gomez, J. E. Acuna, and M. G. Sanchez, "Cellular phone coverage in urban vegetation areas," in *Proc. 3rd Eur. Conf. Antennas Propag.*, Mar. 2009, pp. 2887–2891.
[28] *Antenneregister*. Accessed: Oct. 11, 2024. [Online]. Available: https://www.antenneregister.nl/Html5Viewer/Index.html
[29] *Overview-3DBAG*. Accessed: Sep. 30, 2024. [Online]. Available: https://docs.3dbag.nl/en/
[30] *Nationaal Georegister*. Accessed: Aug. 30, 2024. [Online]. Available: https://nationaalgeoregister.nl/geonetwork/srv/dut/catalog.search#/metadata/3659cae2-29bf-49af-bd8d-737a0bb3dd42
[31] *OVL Utrecht|Datacatalogus Van Utrecht*. Accessed: Sep. 6, 2024. [Online]. Available: https://data.utrecht.nl/dataset/openbare-verlichting
[32] G. Ziegelberger, R. Croft, M. Feychting, A. C. Green, A. Hirata, G. d'Inzeo, K. Jokela, S. Loughran, C. Marino, S. Miller, G. Oftedal, T. Okuno, E. van Rongen, M. Röösli, Z. Sienkiewicz, J. E. H. Tattersall, and S. Watanabe, "Guidelines for limiting exposure to electromagnetic fields (100 kHz to 300 GHz)," *Health Phys.*, vol. 118, no. 5, pp. 483–524, 2020. [Online]. Available: https://journals.lww.com/10.1097/HP.0000000000001210
[33] OpenStreetMap Contributors. (2017). *Map-tile Data Retrieved From*. [Online]. Available: https://www.openstreetmap.org
[34] C. Desset, B. Debaillie, and F. Louagie, "Modeling the hardware power consumption of large scale antenna systems," in *Proc. IEEE Online Conf. Green Commun. (OnlineGreenComm)*, Nov. 2014, pp. 1–6. [Online]. Available: https://ieeexplore.ieee.org/document/7114430
[35] B. Thors, A. Furuskär, D. Colombi, and C. Törnevik, "Time-averaged realistic maximum power levels for the assessment of radio frequency exposure for 5G radio base stations using massive MIMO," *IEEE Access*, vol. 5, pp. 19711–19719, 2017. [Online]. Available: https://ieeexplore.ieee.org/document/8039290/?arnumber=8039290
[36] S. Shikhantsov, A. Thielens, S. Aerts, L. Verloock, G. Torfs, L. Martens, P. Demeester, and W. Joseph, "Ray-Tracing-Based numerical assessment of the spatiotemporal duty cycle of 5G massive MIMO in an outdoor urban environment," *Appl. Sci.*, vol. 10, no. 21, p. 7631, Oct. 2020. [Online]. Available: https://www.mdpi.com/2076-3417/10/21/7631
[37] Gurobi Optimization, LLC. (2024). *Gurobi Optimizer Reference Manual*. [Online]. Available: https://www.gurobi.com
[38] M. Deruyck, E. Tanghe, D. Plets, L. Martens, and W. Joseph, "Optimizing LTE wireless access networks towards power consumption and electromagnetic exposure of human beings," *Comput. Netw.*, vol. 94, pp. 29–40, Jan. 2016. [Online]. Available: https://www.sciencedirect.com/science/article/pii/S1389128615004727
[39] *What is 5G|Everything You Need to Know About 5G 5G FAQ Qualcomm*. Accessed: Sep. 2, 2024. [Online]. Available: https://www.qualcomm.com/5g/what-is-5g
[40] L. Appolloni and D. D'Alessandro, "Housing spaces in nine European countries: A comparison of dimensional requirements," *Int. J. Environ. Res. Public Health*, vol. 18, no. 8, p. 4278, Apr. 2021. [Online]. Available: https://www.mdpi.com/1660-4601/18/8/4278
[41] M. M. Tamasala, S. Shikhantsov, M. Deruyck, E. Tanghe, D. Plets, S. K. Goudos, L. Martens, and W. Joseph, "Combined ray-tracing/FDTD and network planner methods for the design of massive MIMO networks," *IEEE Access*, vol. 8, pp. 206371–206387, 2020. [Online]. Available: https://ieeexplore.ieee.org/document/9246544/?arnumber=9246544
[42] S. Kuehn, S. Pfeifer, and N. Kuster, "Total local dose in hypothetical 5G mobile networks for varied topologies and user scenarios," *Appl. Sci.*, vol. 10, no. 17, p. 5971, Aug. 2020. [Online]. Available: https://www.mdpi.com/2076-3417/10/17/5971

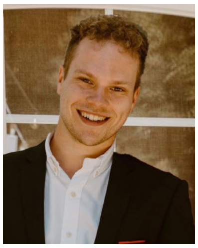

JORN SCHAMPHELEER received the M.Sc. degree in industrial engineering from Ghent University (UGent), Ghent, Belgium, in 2023, where he is currently pursuing the Ph.D. degree. In July 2023, he started as a Research Assistant with the Department of Information Technology, WAVES Research Group. His scientific work is focused on network planning and more specifically on machine learning for network planning in mobile communication networks.

ANKE HUSS is an Associate Professor in environmental epidemiology with a special focus on the spatial distribution of environmental exposures. She is involved in advanced methods of exposure assessment, including modeling various exposures, such as electromagnetic fields, pesticides, noise, and others. She has assessed the effects of these exposures in relation to a wide range of outcomes, including sleep quality, neurodegenerative, and neurological developmental effects, using various research methods, such as case-control and cohort studies. She is a Co-PI of the Dutch LIFEWORK cohort and a member of the Expert Committees ICNIRP and SSM. She is also a member of the Dutch Health Council.

MARGOT DERUYCK (Member, IEEE) received the M.Sc. and Ph.D. degrees in computer science engineering from Ghent University, Belgium, in 2009 and 2015, respectively. Since 2009, she has been a member of the WAVES Group, Department of Information Technology, Ghent University. She became an Assistant Professor in advanced network planning for (beyond) 5G and IoT applications, in 2021. Her scientific work focuses on green wireless access networks (minimal power consumption/human exposure), UAV-based wireless network design and animal Internet of Things (IoT). She is the Science Communication Coordinator of the EU COST CA20120 INTERACT action, the Awards/Membership Elevation and Recognition Office of the IEEE Benelux Section and a panelist for the Swedish-Norwegian Institute for Equine Research. She was part of the organizing committee of various IEEE conferences, such as ISWCS 2017, IEEE PIRMC 2018, and IEEE ICC 2023.